ELSEVIER

Journal of Magnetism and Magnetic Materials 154 (1996) 301–320

journal of magnetism and magnetic materials

Exchange-coupled MBE-grown Co/Cu/Co(111) trilayers

A.J.R Ives [a], J.A.C. Bland [a,*], T. Thomson [b], P.C. Riedi [b], M.J. Walker [c], J. Xu [c], D. Greig [c]

[a] *Cavendish Laboratory, University of Cambridge, Madingley Road, Cambridge CB3 0HE, UK*
[b] *Department of Physics and Astronomy, University of St. Andrews, North Haugh, St. Andrews, Fife KY16 9SS, UK*
[c] *Department of Physics, University of Leeds, Leeds LS2 9JT, UK*

Received 3 July 1995; revised 20 October 1995

Abstract

It is shown that the high-field curvature in the in-plane and polar magnetization curves of exchange-coupled MBE-grown Co/Cu/Co(111) structures can be accurately fitted by assuming a sizeable biquadratic coupling in addition to the bilinear coupling, and the existence of a large areal fraction of ferromagnetic inclusions. Measurements on a sample with a single Co layer confirm that the curvature does not originate from the individual Co layers. Analysis of two Co/Cu/Co(111) trilayers with different Co–Cu interface qualities, as measured by NMR, shows significantly higher bilinear and biquadratic coupling strengths for the trilayer with the better defined Co–Cu interfaces. While NMR indicates reasonably good structural quality on a short lateral length scale, polar Kerr measurements as a function of interlayer thickness, and polarized neutron reflection measurements, indicate the existence of structural imperfections on a long lateral length scale.

Keywords: Anisotropy; Biquadratic coupling; Co/Cu; Exchange coupling; Interface quality; Kerr effect; MBE; NMR; Trilayer

1. Introduction

Interlayer exchange coupling in magnetic multilayers has recently become the subject of intense research. The Co/Cu(111) system has received much attention due to the exceptionally large giant magnetoresistance (GMR) values obtained for it [1,2], and also as a result of important differences in GMR, exchange coupling, and magnetization behaviour which have emerged between those structures grown by sputtering and those grown by molecular beam epitaxy (MBE). The maximum GMR values have been notably smaller in the MBE-grown samples, suggesting that the interface structure strongly influences the coupling strength [3]. Moreover, oscillatory exchange coupling has been found to be much more difficult to observe in Co/Cu(111) films grown by MBE than in equivalent films grown by sputtering [4–10]. The particular type of buffer structure and substrate used to grow MBE multilayers has been shown to have a significant effect on the quality of the Co–Cu interfaces, and to strongly influence the maximum GMR values obtained. Thomson et al. [11] used nuclear magnetic resonance (NMR) to demonstrate that a progressive increase in the GMR of MBE Co/Cu(111) multilayer films grown on Cu/Co/Ge/GaAs, Cu/Au/Co/Ge/GaAs and Cu/Nb/sapphire, in ascending order of GMR values, was associated with a corresponding improvement in the Co–Cu interfacial quality. Studies of the coupling and the magnetization behaviour in

* Corresponding author. Fax: +44-1223-350266; email: jacb1@phy.cam.ac.uk.

SSDI 0304-8853(95)00621-4

Co/Cu(111) films grown on Cu/Au/Co/Ge/GaAs and Cu/Nb/sapphire substrates, as reported here, are therefore important for interpreting the results of the GMR measurements.

In-plane and polar Kerr effect measurements at 300 K have been combined in order to obtain the bilinear and biquadratic coupling strengths at the AFM coupling maxima in two Co/Cu/Co(111) trilayers with wedged Cu(111) interlayers. These two samples, one grown on Cu/Au/Co/Ge/GaAs(110) and one on Cu/Nb/sapphire($11\bar{2}0$), were analysed with the polar Kerr effect for a range of Cu interlayer thicknesses, and then using NMR at 4.2 K to determine the quality of the Co–Cu interfaces. In order to better understand the results from the Cu-wedged trilayers, a single Co(111) layer grown on Cu/Au/Co/Ge/GaAs(110) was studied using in-plane and polar Kerr measurements, and also with polarised neutron reflection (PNR). In addition, it was important to know the effect on the NMR data of the Co seed layer in the Cu-wedged trilayer on GaAs. Hence a sample consisting of only the Co seed layer grown on Ge/GaAs was also analysed with NMR. All four samples were grown by MBE at the University of Leeds, and were given Au capping layers to reduce the effect of oxidation. The structures of the four samples are shown in Table 1.

Table 1
Structures of the four samples grown (i) Cu wedge on GaAs; (ii) Cu wedge on sapphire; (iii) Co single layer on GaAs; (iv) Co seed layer on GaAs

Sample (i)	(ii)	(iii)	(iv)
Au (13 Å)	Au (20 Å)	Au (20 Å)	Au (30 Å)
Cu (15 Å)	Cu (15 Å)	Cu (15 Å)	**Co (15 Å)**
Co (15 Å)	Co (15 Å)	**Co (15 Å)**	Ge (500 Å)
Cu (0–35 Å)	**Cu (0–35 Å)**	Cu (15 Å)	GaAs (110)
Co (15 Å)	Co (15 Å)	Au (200 Å)	
Cu (15 Å)	Cu (15 Å)	Co (15 Å)	
Au (200 Å)	Nb (50 Å)	Ge (500 Å)	
Co (15 Å)	Sapphire ($11\bar{2}0$)	GaAs (110)	
Ge (500 Å)			
GaAs (110)			

2. Sample preparation

For the sample grown on sapphire, we used a method similar to that of Schreyer et al. [8]. A detailed discussion of their method is also given in Ref. [12]. The substrate was heated to 950°C for growth of a 50 Å niobium buffer layer which has been found to improve the structural quality of the subsequent layers [12]. The Nb was deposited at a rate of 0.8 Å/s and grows as bcc (110) on the $Al_2O_3(11\bar{2}0)$ surface. To maximize the degree of crystallinity of the subsequent layers, the sample temperature was held at 375°C for growth of the first Cu(111) layer on Nb. The sample temperature was then reduced to 30°C for growth of the remaining layers so that diffusion at the Co–Cu interfaces was minimized. The Au(111), Co(111) and Cu(111) layers were deposited at rates of about 0.09, 0.20 and 0.50 Å/s, respectively, at a growth pressure of about 5×10^{-10} mbar.

For the samples grown on GaAs, we used a method similar to that of Clarke et al. [13]. The substrate was heated to 600°C before growth to drive off impurities. The sample temperature was reduced to 500°C for growth of a 500 Å germanium buffer layer to provide a well-ordered, smooth surface for subsequent film growth. The Ge was deposited at a rate of 0.15 Å/s and grows as bcc (110) on the GaAs(110) surface. The sample temperature was then further reduced to 100°C for growth of the remaining layers. A 15 Å Co layer was grown directly on the Ge in order to help bridge the (110) orientation of the Ge with the (111) orientation of the layers above [13]. Growth of the Co layer was followed by a 200 Å Au(111) buffer layer, and then the structure of interest. The Au(111), Co(111) and Cu(111) layers were deposited at rates of 0.07, 0.20 and 0.20 Å/s, respectively, at a growth pressure of about 1×10^{-10} mbar.

Reflection high-energy electron-diffraction (RHEED), low- and high-angle X-ray and NMR measurements, performed on similar samples grown in the same MBE system on sapphire and GaAs, indicate (111) growth with flat interfaces for layers including and above the first Cu and first Au layers, respectively [3,11,14]. Scanning tunnelling microscopy (STM) measurements, which have previously shown the tendency for island growth of Co(111) on Cu(111), are described in Section 3.2.

STM measurements performed on the buffer/substrate structure Au/Co/Ge/GaAs(110), grown at Leeds using the same method as that used to produce the GaAs samples studied here, are discussed in Section 8. Thomson et al. [15] have shown using NMR measurements that, at least for films grown on sapphire, the Co(111) layer sandwiched by Cu(111) retains the Cu fcc structure up to thicknesses of the order of 60 Å, while the hcp structure tends to be favoured for greater thicknesses. As mentioned above, the NMR work by Thomson et al. [11] has previously revealed better quality Co–Cu interfaces for MBE-grown Co/Cu(111) multilayers grown on sapphire than those grown on GaAs. In this paper, however, the NMR measurements are seen to reveal better quality interfaces for the trilayer on GaAs than for the sample on sapphire.

3. In-plane magnetization behaviour

In-plane Kerr measurements were carried out in the longitudinal geometry using a 50 mW polarized He–Ne laser beam, a commercial intensity stabilizer, and an electromagnet capable of fields up to 12 kOe. In the Kerr experiments on the samples grown on GaAs, the Co seed layer contributes very little to the overall Kerr rotation. This is due to the presence of the thick 200 Å Au layer and to the limited penetration depth of the laser beam, and to the fact that the Co seed layer is only partially magnetic.

3.1. Single Co layer on GaAs

For the single Co(111) layer on GaAs, in-plane Kerr magnetization curves have been measured to fields in excess of 10 kOe for in-plane field angles of 0°, 45°, 90° and 135° relative to the sample edge. The curve for an in-plane field angle of 0°, shown by the solid line in Fig. 1(a), has a saturation field of about 2.0 kOe and a remanent magnetization $M_r = 0.91 M_s$. The curves for the other three angles are very similar to Fig. 1(a), with saturation fields of the same value within an experimental error of 0.5 kOe, suggesting that the in-plane anisotropy field in this sample is small (≤ 0.5 kOe). A calculation of the in-plane anisotropy of a (111) fcc Co layer shows that the contribution from the first-order cubic magnetocrystalline anisotropy constant K_1 cancels out. The result is an in-plane anisotropy energy with sixfold symmetry of the form

$$K_{an} = K_{sixfold} \cos 6\theta = (K_2/108) \cos 6\theta,$$

where K_2 is the second-order cubic magnetocrystalline anisotropy constant and θ is the in-plane applied field angle. The values of the cubic anisotropy constants for bulk fcc Co are given in Ref. [16] as $K_1 = -0.073$ MJ m^{-3} and $K_2 = -0.018$ MJ m^{-3}, leading to $K_{sixfold}/\mu_0 M = -103$ A m^{-1} (1.3 Oe), which implies an extremely small variation with sixfold symmetry of the in-plane saturation field with applied field angle. A small sixfold anisotropy contribution has recently been observed using ferromagnetic resonance by Schreiber et al. [17] in Co/Cu(111) superlattices grown by MBE on Cu/Nb/sapphire; they suggest that the observation of a sixfold anisotropy in a particular sample implies good structural quality. Fitting of the polar magneti-

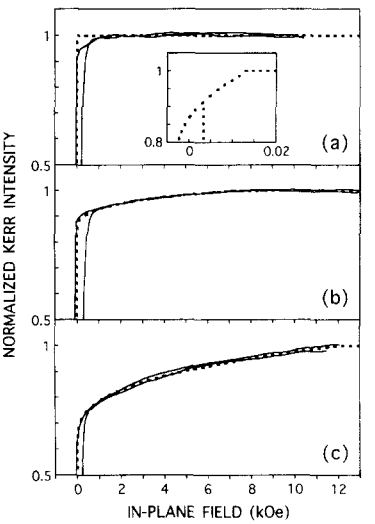

Fig. 1. In-plane Kerr magnetization curves from: (a) the single Co(111) layer on GaAs; (b) the Cu-wedged trilayer on sapphire at a Cu thickness where the exchange coupling is at its largest and antiferromagnetic, but smaller in magnitude than for the Cu-wedged trilayer on GaAs; (c) the Cu-wedged trilayer on GaAs at a Cu thickness where the exchange coupling is at its largest and antiferromagnetic. The dashed lines in (a), (b) and (c) are fits which have been calculated using a coherent rotation model for magnetization reversal, and using the same parameters as the fits for the polar magnetization curves (a), (b) and (c), respectively, in Fig. 4. The inset in (a) shows the detail of the fitted curve at low field.

zation curve from the single Co layer using a coherent rotation model for magnetization reversal, discussed later, suggests that the cubic anisotropy constants in the Co(111) films studied here may be smaller than those from Ref. [16], having values $K_1 = -0.020$ MJ m^{-3} and $K_2 = -0.005$ MJ m^{-3}, which would lead to $K_{\text{sixfold}}/\mu_0 M$ having a still smaller value. Assuming these smaller values of K_1 and K_2 and a coherent rotation model, in-plane magnetization curves have been calculated for the single Co layer. There is a small variation of the shape of these curves with in-plane field angle. The easy-axis curve has a remanence of $M_r = 1.0M_s$. The hard-axis curve, shown by a dashed line in Fig. 1(a) and in the inset of Fig. 1(a), has a remanence of $M_r = 0.87M_s$, which is quite close to that of the experimental curve, but has a saturation field of only 14 Oe, which is two orders of magnitude smaller than the observed saturation field. Even if the values of K_1 and K_2 given in Ref. [16] are used, the saturation field is still only 51 Oe, suggesting that the saturation field of 2.0 kOe observed experimentally is not caused by the cubic anisotropy.

The magnetization curves up to high field could not be obtained with sufficient accuracy to allow small changes in the in-plane saturation field to be discerned. Hence a detailed measurement was made at smaller in-plane fields of the variation of the coercivity of the in-plane magnetization curves with field angle. These results are shown in Fig. 2(a), where the in-plane coercive field, H_c, is plotted as a function of the angle between the in-plane applied field and the sample edge. Almost no variation of coercive field with angle is observed. A fourfold plus a twofold symmetry does exist, however, which can be seen more clearly by subtracting a constant arbitrary field from the data, and plotting the quantity $H' = H_c - 23$ Oe, as shown in Fig. 2(b). The amplitude of the fourfold plus twofold variations in coercive field can be seen from Fig. 2(b) to be only 2 Oe. Thus the experimentally observed 2 Oe variation in coercivity, and the fact that no variation in the in-plane saturation field was observed (within the experimental error of 0.5 kOe), lead to the conclusion that the size of the anisotropy field must be very small, and in any case less than 0.5 kOe.

Using a coherent rotation model, and the values of K_1 and K_2 derived from the perpendicular magnetization curve, the expected behaviour of the coercive field is plotted in Fig. 2(c), which, in contrast with the experimental data, shows sharp peaks and a clear sixfold symmetry. The fact that a sixfold symmetry is not observed experimentally, and that instead a small fourfold plus twofold symmetry is seen, implies that the structure of the Co film in this sample deviates from the ideal structure that one would expect of a perfect (111)-oriented fcc Co film.

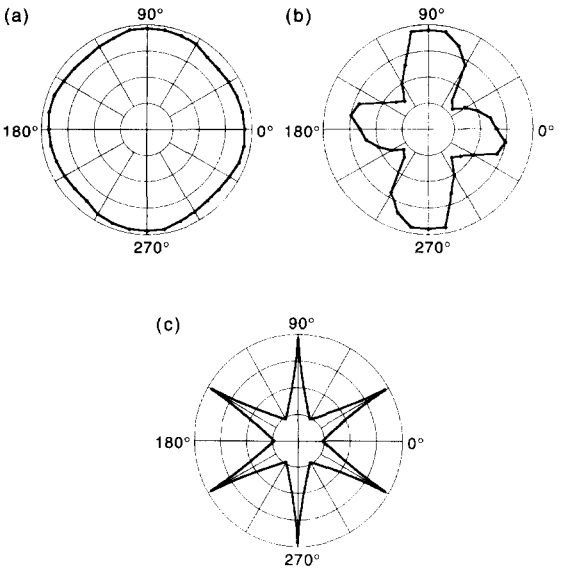

Fig. 2. (a) The in-plane coercive field, H_c, plotted as a function of the angle between the in-plane applied field and the sample edge for the single Co(111) layer on GaAs. The limits of the field scale are 0–27 Oe. (b) The quantity $H' = H_c - 23$ Oe plotted against the same angle. The limits of the field scale are 0–3.2 Oe. This plot shows more clearly the four-fold symmetry in H_c. (c) The calculated variation of the coercive field with in-plane field angle for (111)-oriented Co layers. The limits of the field scale are 0–15 Oe.

A simple coherent rotation model is not an accurate way of predicting coercive fields for this type of sample, however, because of domain formation within the Co layer, and it is therefore not surprising that the calculated coercive fields do not match the experimental coercive fields very well. Also, with such a rapid calculated variation in coercive field with applied field angle, it would only require a small relative misorientation of different crystallites within the film to cause the sixfold variations to be washed out completely into a uniform coercive field

for all angles. The experimental observation of a fairly uniform coercive field with in-plane field angle might therefore indicate that the film quality is reasonably good, in the sense that, for example, no large in-plane uniaxial anisotropies have been caused by the particular growth technique used, or by inclusions of hcp Co with c-axes in the film plane. It must be remembered, though, that a strongly polycrystalline film would also exhibit a uniform coercivity with in-plane field angle.

3.2. Cu-wedged trilayers

The in-plane magnetization curves of exchange-coupled MBE-grown Co/Cu(111) films are not well understood, and exhibit strikingly different behaviour from other coupled structures [5–9]. The unusual features of the in-plane magnetization curves are the high remanences occurring for strongly AFM-coupled films where zero remanence would normally be expected, and a non-linear asymptotic approach to saturation extending to high fields. The high-field in-plane magnetization curve of the single uncoupled Co(111) layer, shown in Fig. 1(a), may be compared with those of the two Cu-wedged Co/Cu/Co(111) trilayers at the first AFM coupling maxima, the positions of which were determined using polar Kerr measurements discussed later. Since the Co layer thickness is nominally the same for all three samples, differences in the shapes of their in-plane magnetization curves can be attributed to coupling effects. The in-plane magnetization curve from the trilayer on sapphire at the first AFM coupling maximum is shown by the solid line in Fig. 1(b), and that from the trilayer on GaAs at the first AFM coupling maximum is shown by the solid line in Fig. 1(c). All the curves are seen to display a significant remanence. The large remanence of $M_r = 0.91 M_s$ and low saturation field of 2.0 kOe for the single Co layer were expected since coupling is absent from this sample.

Neglecting in-plane anisotropies, theory predicts that with the introduction of purely bilinear AFM coupling, acting uniformly across the sample at the relevant Cu thickness, the saturation field will increase, the remanence will go to zero, and the approach to saturation will be linear. The trilayer on sapphire displays a maximum in-plane saturation field of 8 kOe, which is higher than that for the single Co layer, suggesting that significant exchange coupling is present. The remanence of $M_r = 0.88 M_s$ is lower than that for the single Co layer, but is not consistent with uniform AFM coupling across the sample at the relevant Cu thickness, while the curvature in the approach to saturation does not appear to be compatible with purely bilinear exchange coupling.

The trilayer on GaAs displays a maximum in-plane saturation field of 12 kOe, which is higher than that for the trilayer on sapphire, suggesting that even stronger exchange coupling is present. The remanence of $M_r = 0.62 M_s$ is much lower than that for the trilayer on sapphire, but is still not consistent with uniform AFM coupling across the sample at the relevant Cu thickness, while the curvature in the approach to saturation is even greater, which again does not appear to be compatible with purely bilinear exchange coupling.

The shapes of the in-plane magnetization curves from the Cu-wedged trilayers at the AFM coupling maxima are similar to those observed by other groups for Co/Cu(111) trilayers and multilayers [5–9]. To explain the large remanences, it has been suggested that a large areal fraction of the sample consists of regions that are extrinsically ferromagnetically coupled, with the remaining area of the sample consisting of regions that are intrinsically exchange-coupled only [5–10]. These extrinsically ferromagnetically coupled regions are thought to arise as a result of pinholes in the Cu interlayer which become filled by Co during growth of the upper Co layer. The resulting ferromagnetic bridges in these regions then lead to an extrinsic ferromagnetic coupling between the Co layers which dominates over intrinsic antiferromagnetic exchange coupling, and results in the region being ferromagnetically coupled overall. It has been suggested that the bridges across the Cu layer may arise from narrow channels between non-touching neighbouring Cu islands [10], and it has been found by Figuera et al. [18] using STM that Co(111) grows initially on Cu(111) in the form of triangular bilayer islands 150 Å wide. These islands grow with two different stacking sequences so that neighbouring islands with different stacking sequences do not coalesce, forming grain boundaries between them. The grain boundaries are expected to persist during

the growth of Cu(111) on top of the Co film, but since there is no reason for the grain boundaries to coincide from Cu to Co layers, the next Co layer may contact the first one in several places forming magnetic bridges [18].

4. Polar magnetization behaviour

Further insight into the magnetization behaviour of exchange-coupled MBE-grown Co/Cu(111) films may be obtained by magnetizing the Co films perpendicular to their surface. For the 15 Å Co layers in the samples studied here this is a hard direction of magnetization which therefore requires the use of large applied magnetic fields. The approach to saturation is also asymptotic in the polar magnetization curves for the Cu-wedged trilayers. Because the film normal is a hard-axis, however, the analysis of the polar Kerr magnetization curves is simplified by the fact that magnetization can nearly always be assumed to proceed by coherent rotation, and by the fact that the remanence is always zero or almost zero.

The experimental arrangement for the polar Kerr measurements, which were carried out using a 70 kOe superconducting magnet, is shown in Fig. 3 [19]. The sample was placed at the end of an insert tube, close to the centre of the magnet, at room temperature. The He–Ne laser beam was focused on the sample down to a spot size of 0.2 mm at near normal incidence, and moved across it using a plane and a concave mirror both mounted on a micrometer

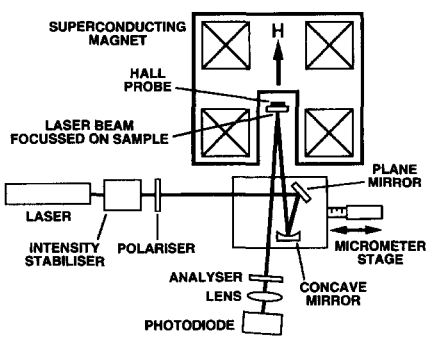

Fig. 3. The experimental arrangement for the polar Kerr measurement. The direction of the magnetic field within the magnet is shown by an arrow.

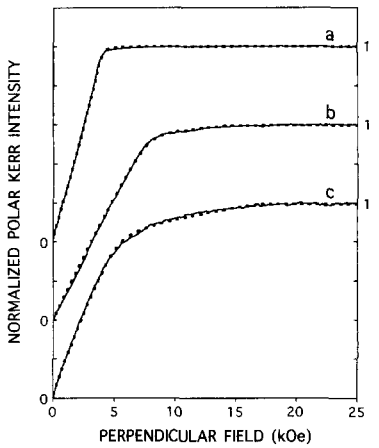

Fig. 4. Polar Kerr magnetization curves from: (a) the single Co(111) layer on GaAs; (b) the Cu-wedged trilayer on sapphire at a Cu thickness of 8.8 Å, where the exchange coupling is at its largest and antiferromagnetic, but smaller in magnitude than for the Cu-wedged trilayer on GaAs; (c) the Cu-wedged trilayer on GaAs at a Cu thickness of 7.4 Å, where the exchange coupling is at its largest and antiferromagnetic. The curves are displaced vertically for clarity. The dashed lines in (a), (b) and (c) are fits which have been calculated using a coherent rotation model for magnetization reversal, and using the same parameters as the fits for the in-plane magnetization curves (a), (b) and (c), respectively, in Fig. 1.

stage. This geometry was designed so that the laser light did not pass through any windows or lenses in the vicinity of the field, thus eliminating problems due to Faraday rotation or birefringence. Polar Kerr measurements were performed at one position on the single Co layer on GaAs, and as a function of position along each wedge for the two Cu-wedged trilayers. Nearly all the perpendicular magnetization curves obtained using the polar Kerr effect have a background contribution which varies linearly with field, and which is always subtracted off before the curves are normalized to the saturation value of the magnetization. In addition, a very slight distortion of the magnetization curves can occur because the relationship between the intensity recorded after the analysing polariser, and the magnetisation, is not perfectly linear. This distortion is assumed to have a negligible affect on the magnetization curves for the purposes of the analysis carried out here.

The polar magnetization curve for the single 15 Å Co layer on GaAs is shown by the solid line in Fig. 4(a). This is compared with the polar magnetization

curve from the Cu-wedged trilayer on sapphire at a Cu thickness of 8.8 Å, at the first AFM coupling maximum, shown by the solid line in Fig. 4(b), and with that from the Cu-wedged trilayer on GaAs at a Cu thickness of 7.4 Å, at the first AFM coupling maximum, shown by the solid line in Fig. 4(c). As mentioned above, the positions of the AFM coupling maxima were determined from polar Kerr measurements performed as a function of Cu thickness, which are discussed later. The curves are displaced vertically for clarity. The approach to saturation is observed to be fairly abrupt for the curve from the uncoupled single Co layer, with this sample, as expected, having the lowest polar saturation field. The curve from the trilayer on sapphire has a higher polar saturation field than the curve from the single Co layer, and the approach to saturation is more rounded. The curve from the trilayer on GaAs has the highest polar saturation field, and the approach to saturation is the most rounded of all the curves. The approach to saturation for the polar magnetization curves from the two trilayers is thus non-linear and asymptotic as it was for the in-plane magnetization curves.

It is found that the initial gradient of the polar magnetization curve from the single Co layer shown in Fig. 4(a) is much greater than the initial gradients of polar magnetization curves from the Cu-wedged trilayers at Cu thicknesses at which the exchange coupling is almost zero, when one would have expected them to be approximately the same. The polar saturation field is affected by the demagnetizing field, interface anisotropy, and strain-induced anisotropies, as well as by the exchange coupling. Differences in the demagnetizing field and in the anisotropies, caused by small variations in film thickness or in the growth procedures, can occur from one sample to the next and are probably the cause of the larger initial gradient of the polar magnetization curve from the single Co layer. Thus, apart from variations in the initial gradient, the observed differences between the shapes of the three polar magnetization curves in Fig. 4 can again be attributed to the effects of coupling, because the Co layer thicknesses are nominally the same in each sample.

5. Calculated magnetization curves

The in-plane magnetization curves and the polar magnetization curves have been simultaneously fitted for the single Co layer and for the Cu-wedged trilayers at the peak of AFM coupling, using a coherent rotation model for magnetization reversal. The fitted curves are shown by dashed lines in Figs. 1 and 4, while the parameters used in the fitting are given in Table 2. This should allow accurate values of maximum coupling strengths to be determined for the Cu-wedged trilayers. It should also help to explain the non-linear asymptotic approach to saturation, which occurs in addition to the large remanence in the in-plane magnetization curves, and also occurs in the polar magnetization curves of the trilayers.

5.1. Fitting curves from the single Co layer

The magnetization curves from the single Co layer were fitted first in order to determine the appropriate values of the cubic magnetocrystalline anisotropy constants K_1 and K_2 to be used in the fitting of the curves from the Cu-wedged trilayers.

Table 2
Parameters used to fit the in-plane magnetization curves in Fig. 1, and simultaneously the polar magnetization curves in Fig. 4, for the Co single layer, the Cu wedge on GaAs at the AFM coupling peak, and the Cu wedge on sapphire at the AFM coupling peak

	Type of region	Fraction (%)	A_{12} (mJ m^{-2})	B_{12} (mJ m^{-2})	B_{12}/A_{12}	$\mu_0 M$ (T)	K_1 (MJ m^{-3})	K_2 (MJ m^{-3})	K_P (MJ m^{-3})	θ_{off}
Co single layer	–	–	–	–	–	1.82	−0.02	−0.005	0.51	1.5°
Cu wedge	EFM	62	0	0	–	1.82	−0.02	−0.005	0.48	5.0°
on GaAs	IE	38	−0.33	−0.165	1/2	1.82	−0.02	−0.005	0.48	5.0°
Cu wedge	EFM	88	0	0	–	1.82	−0.02	−0.005	0.39	2.8°
on sapphire	IE	12	−0.24	−0.08	1/3	1.82	−0.02	−0.005	0.39	2.8°

As discussed above, the cubic anisotropy of the (111) fcc Co layer has a very small effect on the in-plane magnetization curves. In the presence of a demagnetizing field and (a smaller) interface anisotropy field only, the polar magnetization versus field behaviour of the single Co layer would be linear from zero applied field up to saturation. The cubic anisotropy, which in this case has negative sign, causes curvature in the polar magnetization versus field behaviour such that the gradient of the curve increases up to a point near saturation. This curvature can just be observed in the polar magnetization curve from the single Co layer, as shown by the solid line in Fig. 4(a). As mentioned above, the values of $K_1 = -0.020$ MJ m^{-3} and $K_2 = -0.005$ MJ m^{-3} obtained from fitting this polar magnetization curve are smaller than those obtained from Ref. [15].

To fit the polar magnetization curves precisely it was necessary to assume a perpendicular uniaxial anisotropy K_P, which contains a contribution from the interface anisotropy and probably a contribution from magnetoelastic anisotropy. The parameter K_P was then adjusted freely during the fitting procedure. The final value of K_P used in fitting the polar curve from the single Co layer was $K_P = 0.51$ MJ m^{-3}. To obtain a good fit it was also necessary to include an offset θ_{off} in the alignment of the field with the normal to the plane of the sample, which for the single Co layer was $\theta_{off} = 1.5°$. Such offset fields have been observed during polar magnetization measurements on other samples. If the offset angle of the applied field is above a certain value, which is about 5° but varies between samples, small jumps are observed in both calculated and experimental polar curves in the early near-linear increase of the magnetization with field. The effect of the offset is a small amount of rounding of the polar curves in the region of the saturation point, which is, incidentally, far too small to account for the large scale rounding observed in the polar magnetization curves from the Cu-wedged trilayers. The magnetization M has been taken to have the bulk value for fcc Co so that $\mu_0 M = 1.82$ T (see Table 2).

The result of the fitting is that while there is a discrepancy between the calculated and experimental in-plane saturation fields, as discussed above, the agreement between the calculated and experimental polar magnetization curves for the single Co layer is excellent, as is evident from Fig. 4(a).

5.2. Fitting curves from the Cu-wedged trilayers

In fitting the magnetization curves from the Cu-wedged trilayers, it has been assumed that a large areal fraction of the wedges at the relevant Cu thicknesses is extrinsically ferromagnetically coupled (EFM-coupled) as a result of pinholes, with the remaining area intrinsically exchange-coupled (IE-coupled) by bilinear and biquadratic exchange interactions only. The fraction which is EFM-coupled has been taken to be equal to the remanence fraction M_r/M_s for each trilayer. Thus for the Cu-wedged trilayer on sapphire it has been assumed that 0.88 of the area is EFM-coupled and 0.12 of the area is IE-coupled at the Cu thickness at which the AFM coupling is a maximum. For the Cu-wedged trilayer on GaAs it has been assumed that 0.62 of the area is EFM-coupled and 0.38 of the area is IE-coupled at the Cu thickness at which the AFM coupling is a maximum. These assumptions apply to both the polar and in-plane magnetization curves. A bilinear exchange coupling strength A_{12}, where the coupling energy per unit area is equal to $-2A_{12}\hat{M}_1 \cdot \hat{M}_2$, and a biquadratic exchange strength B_{12}, with coupling energy per unit area given by $-2B_{12}(\hat{M}_1 \cdot \hat{M}_2)^2$, were assumed to act between magnetizations M_1 and M_2 in the IE-coupled regions. The EFM-coupled regions were assumed to have $A_{12} \geq 0$ and $B_{12} = 0$.

For each trilayer the in-plane magnetization curve was fitted first by calculating the magnetization curves for the EFM- and IE-coupled regions separately, and then adding them together in the correct ratio. The values of A_{12} and B_{12} obtained for the IE-coupled regions were then used to fit the polar magnetization curve. The values of the cubic anisotropy constants K_1 and K_2 obtained above from fitting the polar magnetization curve of the single Co layer, were used in the fitting of the curves from the trilayers. The various parameters were adjusted until a good fit was obtained for both corresponding in-plane and polar magnetization curves. The final values of K_P used were $K_P = 0.48$ and 0.39 MJ m^{-3} for the trilayers on GaAs and sapphire, respectively, while the final offset angles used were $\theta_{off} = 5.0°$ and 2.8°, respectively (see Table 2).

5.3. Results from fitting the curves of the Cu-wedged trilayers

The calculated curves for the Cu-wedged trilayers are shown as dashed lines in Fig. 1(b) and (c), and Fig. 4(b) and (c); the agreement with the experimental Kerr magnetization curves is excellent. The results of the fitting procedure are the values of the coupling strengths A_{12} and B_{12} obtained for the IE-coupled regions of each trilayer, as shown in Table 2. For the trilayer on GaAs the fitting procedure gives $A_{12} = -0.33$ mJ m^{-2} and $B_{12} = -0.165$ mJ m^{-2}, while for the trilayer on sapphire the fitting gives $A_{12} = -0.24$ mJ m^{-2} and $B_{12} = -0.08$ mJ m^{-2}.

In the presence of biquadratic coupling, the exchange coupling derived from the in-plane saturation field becomes $A_{12} + 2B_{12}$ instead of simply A_{12}, so that it is more accurate to compare the values of $A_{12} + 2B_{12}$ that are obtained here with the values of A_{12} found by other groups from saturation field measurements. The values of $A_{12} + 2B_{12}$ obtained here are $A_{12} + 2B_{12} = -0.66$ mJ m^{-2} for the trilayer on GaAs and $A_{12} + 2B_{12} = -0.40$ mJ m^{-2} for the trilayer on sapphire. Schreyer et al. [8] found a maximum value of $A_{12} = -0.27$ mJ m^{-2} (300 K) for an MBE-grown Co/Cu(111) superlattice, while Johnson et al. [5] found a maximum value of $A_{12} = -0.55$ mJ m^{-2} (300 K) for an MBE-grown Co/Cu(111)/Co wedge. Both of these values of A_{12} were obtained from in-plane saturation fields assuming no biquadratic coupling was present. The values of $A_{12} + 2B_{12}$ obtained here are then clearly in the same range as the values of A_{12} found previously.

The values of the biquadratic coupling strengths obtained here, despite being surprisingly high, thus appear to be the cause of the non-linear curvature in the approaches of the magnetizations to saturation. The value of the ratio of the biquadratic to bilinear coupling is 0.5 for the trilayer on GaAs and 0.33 for the trilayer on sapphire. The higher ratio for the trilayer on GaAs leads to more rounded in-plane and polar magnetization curves at the approach to saturation, as can be clearly seen in Fig. 1(b)–(c) and Fig. 4(b)–(c).

Although the assumption that the fraction of EFM-coupled regions was equal to the in-plane remanence fraction, combined with the values for the coupling strengths given above, gave the best fits to the experimental data, reasonable fits could still be obtained by assuming that some of the remanence resulted from biquadratic coupling. Ignoring in-plane anisotropies, in-plane remanence occurs in the IE-coupled regions when the ratio of biquadratic to bilinear coupling is greater than 0.5. For the in-plane magnetization curve from the trilayer on GaAs it was even possible to obtain an approximate fit by assuming that all of the remanence was due to biquadratic coupling. Biquadratic coupling in the IE-coupled regions can only account for remanence up to the value $M_r/M_s = \sqrt{2}$, however, because large values of the ratio B_{12}/A_{12} result in the magnetizations in adjacent Co layers becoming fixed at 45° to the in-plane applied field direction. Ferromagnetic coupling combined with biquadratic coupling could result in $M_r/M_s > \sqrt{2}$, but in the IE-coupled regions at the Cu thicknesses chosen there is believed to be strong AFM coupling rather than ferromagnetic coupling, which therefore excludes this possibility. Thus a large value for B_{12}/A_{12} cannot account for the large remanence of $M_r = 0.88M_s$ observed for the in-plane magnetization curve from the trilayer on sapphire, and so it seems likely that some or all of the remanence in these trilayers is due to the presence of the EFM-coupled regions. On the basis of this discussion, however, the values of maximum biquadratic coupling strengths given here must be regarded as minimum values.

5.4. Discussion of other work

Bobo et al. [20] used two different methods to fit the in-plane magnetization curves from their Co/Cu multilayers, and one of their curves possessed a shape very similar to that in Fig. 1(c). In the first method, they assumed the multilayers were uniform and did not contain EFM-coupled regions, but assumed the presence of both bilinear and biquadratic coupling terms. They obtained an approximate fit to their magnetization curves with very large values of B_{12} that were up to five times greater than the corresponding values of A_{12}. Such a large ratio of B_{12} to A_{12} was necessary to account for the large remanences observed, but is difficult to understand in the context of the clear bilinear AFM coupling

peaks which have now been observed in samples of this type, and which are observed here also, as described later. Thus the values for the ratio of B_{12} to A_{12} obtained here seem physically more reasonable than those obtained by Bobo et al. using the method just described. The values of B_{12} obtained here are, however, probably still too large to be accounted for by an intrinsic biquadratic coupling effect, since most of the intrinsic theories of biquadratic coupling seem to result in only very small biquadratic coupling strengths [21–23]. It is therefore quite probable that the large values of biquadratic coupling obtained here are extrinsic in origin.

In the second method used by Bobo et al., it was assumed that no intrinsic biquadratic coupling was present, but that the multilayers possessed an array of pinholes with a combined area of about 1% of the total, with the remaining area being AFM-coupled [20]. The pinholes were assumed to influence the orientations of the surrounding spins through the stiffness constant A, which was shown to result in EFM-coupled regions with areas many times greater than those of the pinholes. This effect was also shown to produce the large remanences and curvature in the approach to saturation of the in-plane magnetization curves of their multilayers, with more realistic values being assumed for the bilinear coupling strength. Since it is believed that pinholes do exist in the trilayers studied here, resulting in the existence of the EFM-coupled regions, this effect could provide an alternative explanation to that given in Section 5.2 for the shape of the in-plane magnetization curves obtained from the Cu-wedged trilayers, and possibly also for the shape of the polar magnetization curves.

Closely related to the effect of pinholes studied by Bobo et al., is a model proposed by Gradmann and Elmers [24], who assumed that pinholes and channels in imperfect multilayers affect the finite extension of AFM-coupled regions of the sample in a way that can be modelled theoretically. They calculated the lateral size that an AFM-coupled region of Co/Cu(111) film surrounded by EFM-coupled regions must be in order to remain AFM-coupled. If the size of an AFM-coupled region is below a critical lateral dimension, or if the AFM coupling is lower than a critical value, then it becomes EFM-coupled. A distribution of such AFM-coupled regions of widely differing lateral dimensions could occur, implying that on average a greater proportion of regions would be EFM-coupled, and hence a greater areal fraction of the film would be EFM-coupled, where the AFM coupling strength was smaller.

The model proposed by Gradmann and Elmers is in agreement with the difference observed here in the size of the in-plane remanence observed for the two Cu-wedged trilayers. A higher remanence was observed for the trilayer on sapphire than for the trilayer on GaAs, implying that a greater proportion of the film is EFM-coupled, and both the bilinear and biquadratic coupling strengths were found to be smaller for the trilayer on sapphire. The agreement between this model and the observations made in this study thus supports the original assumption made in Section 5.2 that the remanence fraction is equal to the areal fraction of the sample which is EFM-coupled at the relevant Cu thickness, and does not arise from other sources. If the Gradmann and Elmers model is correct, and if it had been observed here that the trilayer with the higher coupling strength had the higher remanence, then there would have to be another factor contributing to the observed remanence.

The model proposed by Gradmann and Elmers implies that the external applied field necessary to cause ferromagnetic alignment of the two Co layers in a particular AFM-coupled region would depend on the size of the region and on the strength of the AFM coupling within it. Therefore a distribution of regions of differing lateral dimensions, would require a range of different external field strengths in order to ferromagnetically align them. These regions could gradually become ferromagnetically aligned, as the external magnetic field is increased, in such a way as to produce the observed curvature in the approach of the magnetization to saturation. The exact curvature produced would then depend on the distribution of the sizes of the various regions and on how the critical size of a region was related to the applied field. Therefore it seems that, in addition to explaining the differences in remanence, this model could also explain the high-field curvature observed in the magnetization curves of the trilayers studied here.

It has been suggested previously that the curvature in the approach of the magnetization to satura-

tion of the in-plane magnetization curves of MBE-grown Co/Cu(111) multilayers could be due to an in-plane anisotropy contribution rather than to biquadratic coupling [6]. It has been observed that values of the cubic anisotropy constants equal to $K_1 = -0.020$ MJ m^{-3} and $K_2 = -0.005$ MJ m^{-3} are sufficient to accurately fit the polar magnetization curve of the single Co layer, and with the constants at these values the cubic anisotropy has an extremely small effect on the in-plane magnetization curves. Even if K_1 and K_2 were given larger values they would not have the effect on the shape of the in-plane or polar magnetization curves required to cause the observed curvature in the approach of the magnetization to saturation. It has been shown above that the in-plane anisotropy field in the single Co layer is small, and in any case is ≤ 0.5 kOe, which is an order of magnitude smaller than the in-plane saturation fields observed from the Cu-wedged trilayers. These arguments suggest that the anisotropies in an individual Co layer are too small to cause the fairly significant curvature observed, for example, in the magnetization curve from the Cu-wedged trilayer on GaAs at the peak of AFM coupling. An attempt was made to fit the in-plane magnetization curves from the Cu-wedged trilayers using either a uniaxial or a fourfold anisotropy contribution and setting the biquadratic coupling to zero, but it was found to be impossible to fit the data even approximately, despite allowing much larger anisotropies than those observed for the single Co layer. It has been shown, therefore, that anisotropies are not the cause of the curvature observed in the approach to saturation.

Closely related to the discussion of curvature in the magnetization curves of MBE-grown Co/Cu(111) multilayers is the cause of the curvature in plots of magnetoresistance (MR) versus applied field in the same structures. Barlett et al. [25] have shown that the high degree of curvature in the MR versus field dependence of their MBE-grown Co/Cu(111) superlattices, extending to fields well beyond the point at which the magnetization appears to saturate, can be well described by a Langevin-like saturation function. They suggest that such a field dependence results from electron scattering from an assemblage of paramagnetic spins, most likely at the interfaces between the Co and Cu layers. It is therefore a possibility that the curvature in the approach to saturation of the magnetization curves of such structures could result from the gradual alignment of such paramagnetic spins, if they existed. However, the fact that a significant curvature or an asymptotic approach to saturation extending to high fields is not observed in either the in-plane or polar magnetization curves of the single Co layer, tends to rule out this possibility.

6. Variation of polar saturation fields with Cu interlayer thickness

Polar Kerr measurements were performed as a function of Cu interlayer thickness on the Cu-wedged trilayers in order to determine the positions of the AFM coupling maxima for the fitting procedure described above, to determine the period of the oscillations, and to investigate the structural homogeneity of the trilayers. In-plane Kerr measurements were also carried out as a function of interlayer thickness, but the large remanence, asymptotic approach to saturation, and high saturation fields of the in-plane magnetization curves of the Cu-wedged trilayers, made it particularly difficult to reliably determine variations in the in-plane saturation fields as a function of interlayer thickness.

The conventional perpendicular saturation field $H_s^{\perp}$ has been estimated for the Cu-wedged trilayers by taking the intersection of the perpendicular magnetization curve with $M/M_s = \alpha$, where α is chosen to be the highest value of M/M_s at which the values of $H_s^{\perp}$ obtained for all wedged layer thicknesses are not seriously affected by noise in the magnetization curves. This is illustrated for the polar magnetization curve from the trilayer on GaAs at a Cu thickness of 19.1 Å, which is at the second AFM coupling peak, as shown in Fig. 5. For both trilayers, α has been chosen to have the value 0.94. This procedure was necessary because of the asymptotic approach of the magnetization to saturation and because of noise fluctuations in the data, although it does lead to $H_s^{\perp}$ being an underestimate of the true saturation field. A second saturation field $H_s^{\chi\perp} = 1/\chi_0$ has also been defined, where χ_0 is the initial magnetization gradient of the perpendicular magnetization curve (see Fig. 5), and $H_s^{\chi\perp}$ has been used to analyse the magnetization curves from the Cu-

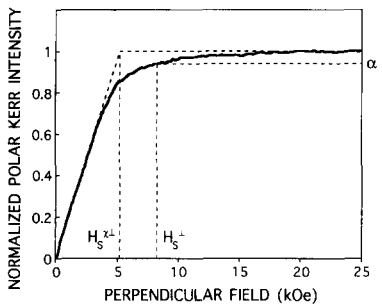

Fig. 5. A polar Kerr magnetization curve from the Cu-wedge on GaAs, corresponding to a Cu thickness of 19.1 Å, at the second peak of antiferromagnetic coupling, with dashed lines showing how $H_s^{\perp}$ and $H_s^{\chi\perp}$ are defined. $H_s^{\perp}$ is obtained from the intersection of the magnetization curve with $M/M_s = \alpha$, where α has been taken to have the value 0.94. $H_s^{\chi\perp}$ is obtained by applying a linear fit to the magnetization curve for -2 kOe $< H < 2$ kOe and then extrapolating this fit to the intersection with $M/M_s = 1$.

wedged trilayer on GaAs. Evaluating this saturation field should in principle allow further information to be extracted from the perpendicular magnetization curve, as its dependence on the quantities that vary with the wedge thickness is somewhat different.

It is possible, using certain assumptions, to obtain general expressions relating the perpendicular saturation fields $H_s^{\perp}$ and $H_s^{\chi\perp}$ to the exchange coupling strengths A_{12} and B_{12}. In the case of non-identical magnetic layers with significantly different interface anisotropy fields, these expressions may in theory be used to extract both the ferromagnetic and AFM bilinear coupling strengths from the perpendicular magnetization curves. The relationship between $H_s^{\perp}$ and A_{12} has been used at Cambridge in an investigation of the ferromagnetic coupling in an Fe/Pd/Fe(001) wedge structure [26]. For the Cu-wedged trilayers studied here, the two Co layers in each trilayer are identical, so that in this case information about the ferromagnetic coupling cannot be obtained by this method.

In the presence of negative bilinear and biquadratic coupling such that $A_{12} \leq 0$ and $B_{12} \leq 0$, the dependence of $H_s^{\perp}$ on A_{12} and B_{12} is given by

$$H_s^{\perp} = -\frac{4}{\mu_0 Md}(A_{12} + 2B_{12}) + H_a^{\perp},$$

where it has been assumed that M and d are equal to the bulk magnetization and the nominal thickness, respectively, of the Co layers. The dependence of $H_s^{\chi\perp}$ on A_{12} and B_{12} for $A_{12} \leq 0$ and $B_{12} \leq 0$ has been calculated assuming that the magnetizations rotate in a plane that includes the surface normal [27]. This is a valid assumption provided that $A_{12} \leq 2B_{12} \leq 0$, giving

$$H_s^{\chi\perp} = -\frac{4}{\mu_0 Md}(A_{12} - 2B_{12}) + H_a^{\chi\perp}.$$

Both of these expressions have been checked using numerical simulations for the type of films studied here. In theory, the quantities $H_a^{\perp}$ and $H_a^{\chi\perp}$ are equal to the conventional and initial gradient saturation fields of the individual magnetic layers of the trilayer in the absence of coupling, and depend on the magnetocrystalline and interface anisotropies of the magnetic layers, and on demagnetizing effects. For an ideal sample these quantities would not be expected to depend on the interlayer thickness, but for the Cu-wedged trilayers studied here $H_a^{\perp}$ and $H_a^{\chi\perp}$ are sample dependent and vary with Cu thickness. The peaks due to exchange coupling are thus superimposed on a large varying background contribution arising from $H_a^{\perp}$ and $H_a^{\chi\perp}$. The background contribution will be sensitive to the quality of the magnetic/non-magnetic interfaces and to the homogeneity of the magnetic layers. Hence, by observing the variations in the background contribution using polar Kerr measurements, insight may be gained into the magnetic layer quality in the Cu-wedged trilayers. Accurate values of the coupling strengths cannot be obtained from the plots of either $H_s^{\perp}$ or $H_s^{\chi\perp}$ versus interlayer thickness because this requires the absolute value of the saturation field to be known.

6.1. Cu-wedged trilayer on GaAs

The results from the polar Kerr measurements on the Cu-wedged trilayer on GaAs are shown in Fig. 6(a), where $H_s^{\perp}$ and $H_s^{\chi\perp}$ are plotted versus Cu interlayer thickness. The plot of $H_s^{\perp}$ shows both the first and second AFM coupling peaks, at about 9 and 20 Å Cu, respectively, in good agreement with previous measurements on MBE-grown Co/Cu(111) structures [8,9]. The plot of $H_s^{\chi\perp}$ shows the peak at 20 Å, but the peak at 9 Å is obscured by a steady increase in $H_s^{\chi\perp}$ towards zero Cu thickness. This

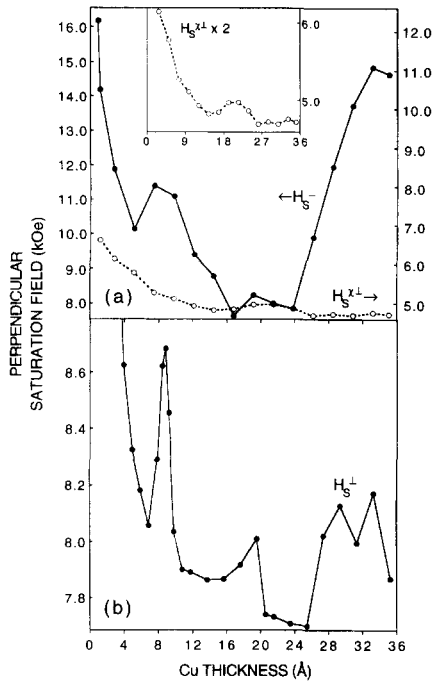

Fig. 6. (a) $H_s^{\perp}$ (closed circles) and $H_s^{\chi\perp}$ (open circles) are plotted versus Cu interlayer thickness for the Cu-wedged trilayer on GaAs. The scale for $H_s^{\perp}$ is on the left hand side of the plot while the scale for $H_s^{\chi\perp}$ is on the right hand side. (b) $H_s^{\perp}$ is plotted versus Cu interlayer thickness for the Cu-wedged trilayer on sapphire.

increase is even greater in magnitude in the plot of $H_s^{\perp}$. As stated above, in addition to being sensitive to the coupling, both perpendicular saturation fields are sensitive to variations in the interface anisotropy field. Thus an explanation for the increases towards zero Cu thickness might be found by noting that $H_s^{\perp}$ and $H_s^{\chi\perp}$ will be significantly greater for a 30 Å Co layer than for two 15 Å Co layers because of the smaller interface anisotropy field in a 30 Å Co layer [13]. Incomplete coverage of the Cu interlayer towards zero Cu thickness, as is known to occur from the STM measurements by Figuera et al. [18], would result in regions in which the Co thickness was 30 Å, alongside regions where two separate 15 Å Co layers existed. Since the laser spot size, 0.2 mm, is orders of magnitude larger than the 150 Å island size observed by Figuera et al., the measured perpendicular magnetization curve would then tend to that of a 30 Å Co layer, causing $H_s^{\perp}$ and $H_s^{\chi\perp}$ to increase towards zero Cu thickness, as observed.

An alternative explanation for the increases towards zero Cu thickness could be that the strength of the interface anisotropy at the Co–Cu interfaces is itself changing in this region. This possibility is suggested by the results of a study by Engel et al. [28] in which a large decrease in the perpendicular saturation field was observed, due to a change in the interface anisotropy, as increasing amounts of Cu(111) were deposited on a 12 Å Co(111) layer that was initially exposed to vacuum. It is interesting that the decrease in the perpendicular saturation field observed by Engel et al. was about 6 kOe at Cu coverages of 0–5 Å Cu, which is almost the same as the 6.1 kOe increase that is observed here in the plot of $H_s^{\perp}$ as the Cu thickness is reduced from 5 to 0.9 Å. It must be remembered, however, that the interface anisotropy in the Co/Cu/Co(111) trilayer system studied here would not be expected to vary in precisely the same way as the interface anisotropy of the Cu/Co(111) system with no top Co layer.

Above 24 Å Cu thickness, $H_s^{\chi\perp}$ flattens out, as expected, but $H_s^{\perp}$ increases rapidly by about 7 kOe. Since $H_s^{\perp}$ and $H_s^{\chi\perp}$ behave differently in this region, and do not both increase, the cause of the large increase in $H_s^{\perp}$ must be different from that proposed above to account for the increases in $H_s^{\perp}$ and $H_s^{\chi\perp}$ towards zero Cu thickness. A variation of the interface anisotropy field in this region of Cu thickness would cause both $H_s^{\perp}$ and $H_s^{\chi\perp}$ to be affected in the same way, and can therefore be ruled out. A variation in the Co magnetocrystalline anisotropy could, however, cause $H_s^{\perp}$ and $H_s^{\chi\perp}$ to diverge significantly. It is of interest to note that the difference between the Co fcc and hcp magnetocrystalline anisotropies is about 6.7 kOe. Thus it might be the case that the observed 7 kOe increase in $H_s^{\perp}$ at the thicker end of the Cu wedge is caused by a volume fraction of the upper 15 Å Co layer growing as hcp Co, with the c-axis easy direction of magnetization directed out-of-plane, in the region of Cu thickness below 24 Å. This would mean that at least the upper Co layer is not homogeneous in the direction in which the Cu thickness changes. It is known from NMR measurements by Mény et al. [29] that the proportion of hcp Co in an fcc Co(111) layer grown on fcc Cu(111) reduces as the thickness of the Cu underlayer increases, as a result of improved reconstruction of the fcc structure of Cu with in-

creasing layer thickness [15]. The amount of hcp Co needed to produce the observed effect might only be as small as 10%. The NMR measurements performed on the Cu wedge on GaAs (see Fig. 7(a)), which are described in more detail below, do not rule out the presence of some hcp content, but do not provide evidence for it either. If some hcp Co were present it would produce a shoulder at 220 MHz to the main fcc Co peak at 214 MHz, with a smaller double peak at 225 MHz [29]. None of these features are observed, but they could be hidden by the broadening of the main fcc peak.

In the region 7–24 Å Cu, the amplitude of the variations in $H_s^{\perp}$ is clearly much greater than the amplitude of those in $H_s^{\chi\perp}$. This is consistent with the sample containing both IE- and EFM-coupled regions. An EFM-coupled region should have a perpendicular saturation field below that of an IE-coupled region. The value of $H_s^{\perp}$ is representative of the saturation field of the IE-coupled regions, so that variations in $H_s^{\perp}$ are unaffected by the EFM-coupled regions. Since $H_s^{\chi\perp}$ represents an average over both types of region, however, variations in $H_s^{\chi\perp}$ are reduced by the presence of the EFM-coupled regions. The decrease in the amplitude of the variations in $H_s^{\chi\perp}$, relative to those in $H_s^{\perp}$, with decreasing Cu thickness, therefore implies that the proportion of EFM-coupled regions increases with decreasing Cu thickness in this sample. This could be caused by increased pinhole coupling between the Co layers with decreasing Cu thickness.

It is possible that some of the variations in the saturation fields arise from changes in the biquadratic coupling strength with Cu thickness. It was found from the fitting of the magnetization curves above, that at the peak of AFM coupling the value of A_{12} was twice that of B_{12}. The expression given above for $H_s^{\chi\perp}$ in terms of A_{12} and B_{12} shows that $H_s^{\chi\perp}$ depends on the quantity $A_{12} - 2B_{12}$, so that the contributions from A_{12} and B_{12} might cancel at this Cu thickness, whereas $H_s^{\perp}$ depends on $A_{12} + 2B_{12}$, for which the contributions add. It is perhaps therefore not surprising that the peak height in $H_s^{\chi\perp}$ is found to be much reduced compared with $H_s^{\perp}$ in the region of the first AFM coupling peak. Above 24 Å Cu thickness, the variation in $H_s^{\chi\perp}$ is also found to be much reduced compared with the large increase in $H_s^{\perp}$, suggesting again the presence of biquadratic coupling. It is difficult, however, to see why the biquadratic coupling should increase to such a high value at this fairly large Cu thickness, given that it is expected from theory and previous experimental work that both intrinsic exchange coupling strengths should decrease rapidly with increasing interlayer thickness.

The period of the coupling determined from $H_s^{\perp}$ is 11 ± 2 Å, which is similar to the periods of 9 and 9.4 Å found in Refs. [8] and [9] respectively. It differs somewhat from the period of 17 Å found in Ref. [10], but this value seems out of line with most of the others. The period obtained here agrees well with the period of 10 Å obtained for the sputtered Co/Cu(111) multilayer in Ref. [1], and is similar to the period of 9.36 Å predicted by Bruno and Chappert using an RKKY theory for the coupling mechanism [30].

6.2. Cu-wedged trilayer on sapphire

The results from the polar Kerr measurements on the Cu-wedged trilayer on sapphire are shown in Fig. 6(b), where $H_s^{\perp}$ is plotted versus the Cu layer thickness. The saturation field $H_s^{\chi\perp}$ has not been plotted because the AFM coupling in this wedge was reduced compared with the wedge on GaAs, and as a consequence no peaks due to the coupling could be observed in $H_s^{\chi\perp}$.

The plot of $H_s^{\perp}$ shows both the first and second AFM coupling peaks, at about 9 and 20 Å Cu respectively, as observed for the Cu-wedged trilayer on GaAs, giving a period for the coupling at again 11 ± 2 Å. The large increase in $H_s^{\perp}$ which occurred towards zero Cu thickness for the wedge on GaAs, also occurs for this sample. There is a significant increase in $H_s^{\perp}$ above about 25 Å Cu thickness, in exactly the same way as an increase was observed in $H_s^{\perp}$ above 24 Å thickness for the wedge on GaAs. This time, however, an increase of about 1.5 kOe is observed in $H_s^{\chi\perp}$ above 25 Å (not shown).

7. Analysis of the NMR data

The usefulness of NMR in determining the interface structure of Co-based multilayers is now well established [31]. We performed ^{59}Co NMR measurements at 4.2 K on both Cu-wedged trilayers; the

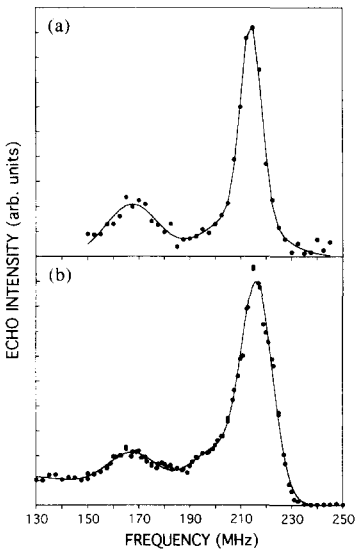

Fig. 7. (a) The ^{59}Co NMR spectrum for the Cu-wedged trilayer on GaAs. The spectrum is characteristic of fcc (111) Co layers having interfaces with fcc (111) Cu. The main peak is centred at 214.3 MHz and is associated with Co atoms within the Co layers which are surrounded by twelve Co nearest neighbours. The smaller peak at 167.4 MHz is associated with Co atoms at the Cu interfaces which are surrounded by nine Co and three Cu nearest neighbours. Intensity between and outside these peaks is due to interfacial mixing. (b) The ^{59}Co NMR spectrum for the Cu-wedged trilayer on sapphire.

results are shown in Fig. 7. The ^{59}Co NMR spectrum was measured in a phase detected, swept frequency spin-echo spectrometer developed at the University of St. Andrews [32]. The samples were placed in a circuit, tuned and matched to the 50 Ω line. At each frequency the echo was integrated and measured at phase angles φ and $\varphi + \pi/2$. The phase insensitive quantity $S = (S_{\varphi}^2 + S_{\varphi+\pi/2}^2)^{1/2}$ was then determined and plotted against frequency, after the usual correction for ω^2, and an additional correction to allow for the variation of spin–spin relaxation time, T_2, across the spectrum [11]. The observed distribution of ^{59}Co resonance frequencies reflects the distribution of effective magnetic fields experienced by the ^{59}Co nuclei, and hence shows the proportion of Co atoms in different atomic environments.

7.1. Cu-wedged trilayer on GaAs

The corrected NMR spectrum from the Cu-wedged trilayer on GaAs is shown in Fig. 7(a). The main NMR peak, centred at 214.3 MHz, is due to the atomic environment where the parent Co atom is surrounded by 12 nearest-neighbour Co atoms, and represents Co atoms within the Co layers. This peak is displaced from the resonance frequency of 217.4 MHz found for fcc Co powder. The displacement is thought to arise from strain associated with the lattice mismatch between Co with lattice constant 3.54 Å and Cu with lattice constant 3.61 Å. Similar strain behaviour has been observed for Co/Cu(111) multilayers [11]. The smaller peak, centred at 167.4 MHz, is due to an atomic environment where three of the nearest-neighbour Co atoms have been replaced by Cu atoms, and represents Co atoms at the interfaces with the Cu [11,29]. This is the ideal interface between fcc Co and fcc Cu with the (111) orientation. Intensity between and outside the two main peaks is then due to atoms in a non-ideal environment, and represents a roughening of the interface, where one or two, or more than three, of the 12 nearest-neighbour Co atoms have been substituted with Cu atoms. It should be noted, however, that the existence of grain boundaries in the films may also lead to a contribution to the intensity between the bulk and ideal interface peaks.

The NMR measurement on the Cu-wedged trilayer on GaAs is sensitive to the 15 Å Co seed layer in addition to the two 15 Å Co layers that form the wedged trilayer. An NMR measurement was therefore done on a sample consisting of just the Co seed layer on Ge/GaAs with a Au capping layer (structure given in Table 1) to determine the effect of the seed layer on the spectrum from the trilayer. No NMR peaks at all were observed from the seed layer, with the echo intensity no higher than the background level, so it was concluded that the contribution of the seed layer to the NMR signal detected from the trilayer was negligible.

The ideal interface and main NMR peaks in Fig. 7(a) were each fitted with a Gaussian function. Comparison of the integrated area under the Gaussian functions associated with the ideal interface and main NMR peaks provides a direct estimate of the ratio of the number of ideal interfacial Co atoms to the number of Co atoms within the Co layers, and thus enables the ratio of ideal to non-ideal interfacial areas to be determined. Using this method it was estimated that of the order of half of the film's total

Co–Cu interfacial area is ideal, with the remaining area roughened by the intrusion of Cu atoms.

7.2. Cu-wedged trilayer on sapphire

The corrected NMR spectrum from the Cu-wedged trilayer on sapphire in Fig. 7(b) shows the main peak at 216.6 MHz, which is significantly closer to the fcc Co powder value of 217.4 MHz, indicating that the Co layers are less strained than in the Cu-wedged trilayer on GaAs. The interface peak occurs at 168.2 MHz, which is close to the frequency observed for the trilayer on GaAs. An important difference, however, is that there is significantly more intensity between the main peak and the interface peak, with a definite shoulder to the main peak appearing at about 195 MHz. A possible explanation for the shoulder at 195 MHz is that it arises from Co atoms where one of the twelve nearest-neighbour Co atoms has been substituted with a Cu atom. The reason the shoulder occurs at 195 MHz, rather than being near the peak position of 199 MHz measured by Le Dang et al. [31] for a dilute Co–Cu alloy, is possibly that the position of the shoulder has been shifted due to strain in the Co layer. The additional intensity between the peaks is a clear indication that the quality of the Co–Cu interfaces is worse than for the trilayer on GaAs. By fitting the data with Gaussian functions it was estimated that of the order of one-third of the film's total Co–Cu interfacial area is ideal, with intermixing between the Co and Cu layers occurring over a larger fraction of the area of the sample than for the Cu-wedged trilayer on GaAs.

7.3. Implications of the NMR data

The NMR measurements have shown that the Co–Cu interfaces are significantly better in the trilayer on GaAs than in the trilayer on sapphire, while fitting of the magnetization curves has shown that A_{12} and B_{12} are significantly larger in magnitude for the Cu-wedged trilayer on GaAs. This is convincing evidence that the exchange coupling in Co/Cu(111) samples is critically dependent on the interface quality at the magnetic/non-magnetic interfaces, and moreover that the size of the coupling increases with an improvement in the interface quality in such samples. These measurements do not imply that the Co–Cu interface quality is generally worse, or that the coupling is generally smaller for structures grown on sapphire than for structures grown on GaAs. This is because variations in growth procedures can easily occur from one sample to the next and result in a wide variation in the quality of the film structure, independently of the type of substrate on which the structure is grown. In fact, the growth pressure was higher for the sample grown on sapphire than for the sample on GaAs, which might have led to a poorer film quality for the trilayer on sapphire. As mentioned above, better Co–Cu interface quality and larger GMR have been observed previously for Co/Cu(111) multilayers grown on sapphire than for similar multilayers grown on GaAs [11].

It was shown above that the trilayer on sapphire possessed a higher in-plane remanence than the trilayer on GaAs at the AFM coupling peak. If the model of IE- and EFM-coupled regions is correct, the higher remanence implies that a greater proportion of the area of the sample consists of EFM-coupled regions, and therefore that a larger number of pinholes per unit area exist in the Cu interlayer at the relevant Cu thickness than in the trilayer on GaAs. A larger number of pinholes per unit area would imply a poorer interface quality for the trilayer on sapphire than for the trilayer on GaAs, which is therefore consistent with the NMR measurements.

The spectra from both Cu-wedged trilayers show more intensity between and outside the two main peaks than spectra obtained previously from Co/Cu(111) multilayers using the same equipment [11], so that the Co–Cu interface quality in these samples is not as good as can be obtained. It has been suggested [33], however, that the NMR spectra from samples with wedged interlayers may be poorer than those from samples with uniform layer thicknesses but with the same Co–Cu interface quality, because pinholes are likely to occur at the thinner end of a wedged layer which can then spoil the spectrum from the whole sample.

8. Analysis of the PNR data

PNR measurements were carried out on the ISIS facility at the Rutherford Appleton Laboratory on the single Co layer on GaAs (structure given in Table 1).

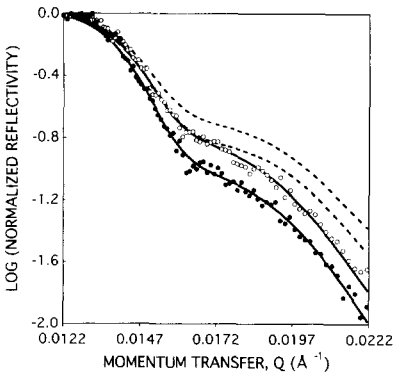

Fig. 8. Polarised neutron reflection data from the single Co layer on GaAs. The logarithms of the normalized up-spin (open circles) and down-spin (closed circles) reflectivities have been plotted for the lower Q values in the range $Q = 0.0122$ to 0.0222 Å^{-1} near the critical edge. The dashed lines show the calculated spin-up and spin-down reflectivities assuming ideal interfaces with no roughness for all layers, and show poor agreement with the data. The solid lines are calculated assuming a significant roughness is present in the layer structure and give much better agreement with the data. The parameters assumed in calculating the solid line curves are given in Table 3.

The sample was placed in a field strong enough to saturate the magnetization in-plane. The neutron beam was incident on the surface of the sample at a grazing angle of $\theta = 0.36°$, with a wavelength λ which was varied from 2 to 6.5 Å. The angle θ was chosen so that the range of reflectivities corresponding to the variation in wavelength included the critical edge, which is the point where the reflectivity starts to deviate from unity as the wavelength decreases. The neutrons were polarized either parallel (up-spin) or antiparallel (down-spin) to the Co magnetization, and the measured reflected intensity, which is different for the up- and down-spin states, was normalized to the incident intensity for each polarization. It is usual to plot the logarithm of the spin-dependent reflectivities against twice the component of the wavevector perpendicular to the sample surface, or momentum transfer, $Q = (4\pi \sin\theta)/\lambda$. In Fig. 8 the logarithms of the normalized up-spin (open circles) and down-spin (closed circles) reflectivities are plotted for the lower Q values in the range $Q = 0.0122$ to 0.0222 Å^{-1} near the critical edge.

The data have been fitted using bulk values of the scattering densities nb obtained from Ref. [34] for the various layers in the sample, where n is the atomic number density and b is the neutron scattering length for each layer. For the magnetic layers an additional scattering parameter $\pm nC\overline{\mu}$ must be added to nb, where $\overline{\mu}$ is the average magnetic moment per atom, C is a constant with value $2.65 \times 10^{-15} m/\mu_B$ if $\overline{\mu}$ is in Bohr magnetons [35], and the positive and negative signs apply for the up- and down-spin states, respectively. It was assumed initially that the upper Co layer possessed the full bulk moment. Since a quantitative Kerr measurement has been performed on the sample consisting of just the Co seed layer, suggesting that the moment of the Co seed layer was reduced to about 1/8 of that of a 'normal' Co layer, it was initially assumed that the seed layer in this sample possessed 1/8 of the bulk moment.

We found that it was possible to obtain good agreement between the calculated reflectivities and the data in this region of Q values by assuming that a significant roughness was present in the layer structure, as shown by the solid curves in Fig. 8. The fitted parameters used to produce the solid curves are shown in Table 3. The roughness was fitted for the air–film interface and for the Ge layer, but this is not a unique solution. A more equal distribution of roughness over the various layers is more likely and could also be used to fit the data. If ideal interfaces are assumed for all layers, calculated reflectivities are obtained which do not have the correct magnitude as shown by the dashed curves in Fig. 8.

The nominal thicknesses were adequate for fitting

Table 3
Parameters used in the fitting of the neutron reflectivities for the Co single layer, shown by the solid curves in Fig. 8

Medium	Thickness (Å)	Scattering density nb (10^{-6} Å^{-2})	$nC\overline{\mu}$ (10^{-6} Å^{-2})	Fitted roughness (Å)
Air	–	0	0	64 (air–film)
Au	20	4.659	0	0
Cu	15	6.538	0	0
Co	15	2.236	3.256 (4.140)	0
Cu	15	6.538	0	0
Au	202.7 (200)	4.659	0	0
Co	15	2.236	0.092 (0.517)	0
Ge	408.9 (500)	3.625	0	47
GaAs	–	3.071	0	–

the data, except in the case of the thicker Au layer and the Ge layer for which different thicknesses were needed to fit the data, and for which the nominal thicknesses are shown in brackets in Table 3. The large difference between the nominal and fitted thicknesses for the Ge layer was permissible because of a large uncertainty in the Ge thickness that was grown for this particular sample. The nominal scattering densities nb were unchanged after fitting, while the values of $nC\overline{\mu}$ for the upper Co layer and the Co seed layer were both reduced by the fitting, with the initial nominal values shown in brackets. The reductions in $nC\overline{\mu}$ are not an accurate indication of the size of the moment in these layers because the spin-dependent reflectivities at high Q have not been fitted.

The fitting procedure for the PNR data does not allow the lateral length scale of the roughness in the plane of the sample to be deduced. From the PNR data alone it is therefore impossible to say whether the roughness that is observed is on a short length scale comparable with the 15 Å layer thickness of the upper Co layer, or whether it is on a very long length scale comparable with the width of the sample. Since NMR data on the Cu-wedged trilayers showed reasonably good interfaces on a short lateral length scale, the observation of a significant roughness using PNR thus points to a structural quality which is poor over a long lateral length scale. The existence of a significant roughness is consistent with the observation by Figuera et al. of 150 Å islands for the growth of Co(111) on Cu(111) leading to pinholes in the Cu [18]. Roughness may also arise from the buffer/substrate structure in the samples grown on GaAs. STM measurements have been carried out on the buffer/substrate structure Au/Co/Ge/GaAs(110) grown at Leeds using the same method as that used to produce the GaAs samples studied here [36]. These measurements suggested that growth occurs with islands approximately 200 Å wide with narrow channels about 20 Å deep between them. The roughness may also explain the occurrence of the features observed in the plots of the polar saturation fields versus Cu thickness on the Cu-wedged trilayers, which could not be attributed to exchange coupling, and which implied the existence of structural imperfections varying on a long lateral length scale.

9. Conclusions

The main results obtained for the MBE Co/Cu(111) system can be summarised as follows:

(i) In-plane measurements on the single Co layer on GaAs showed very little in-plane anisotropy, while the small amount that was observed showed a fourfold plus a twofold behaviour. No evidence of the expected sixfold symmetry was found, suggesting non-ideal Co growth. Comparison of the in-plane and polar magnetization curves of the single Co layer with those of the Cu-wedged trilayers at the maximum of the AFM coupling showed that the high-field curvature in the in-plane and polar magnetization curves from the Cu-wedged trilayers does not originate from the individual Co layers.

(ii) The high in-plane remanence observed in the magnetization curves of even strongly AFM-coupled regions of both Cu-wedged trilayers was attributed to ferromagnetic pinhole coupling through the Cu interlayer. It was found that the in-plane and polar magnetization curves from the trilayers could be accurately fitted by dividing the film into EFM-coupled regions and IE-coupled regions, and assuming firstly that the remanence fraction was equal to the areal fraction of the film that was EFM-coupled, and secondly that a sizeable biquadratic coupling strength in addition to the bilinear coupling existed in the IE-coupled regions.

(iii) The maximum coupling strengths obtained for the trilayer on GaAs, $A_{12} = -0.33$ mJ m^{-2} and $B_{12} = -0.165$ mJ m^{-2}, were found to be significantly larger than those obtained for the trilayer on sapphire, $A_{12} = -0.24$ mJ m^{-2} and $B_{12} = -0.08$ mJ m^{-2}. Comparison of the exchange coupling strengths in terms of the in-plane saturation field $A_{12} + 2B_{12}$, with A_{12} derived from saturation fields in other work, showed that the values obtained here were in the same range as those found previously. It was noted that higher values of biquadratic coupling strength could also have been used to give an approximate fit to the data.

(iv) Although a proportion of the in-plane remanence could also be accounted for by higher values of biquadratic coupling, it was noted that the highest remanence could not be totally accounted for assuming biquadratic coupling alone. Attributing the remanence fraction to the proportion of EFM-coupled

regions rather than to other causes was found to be in agreement with a consideration of the critical size of an AFM-coupled region suggested by Gradmann and Elmers [24], thus lending support to the assumptions made here. In-plane remanence could also be accounted for using the model suggested by Bobo et al. [20] based on pinholes.

(v) The biquadratic coupling term accounted for the significant curvature observed in the approach of the magnetization to saturation for both in-plane and polar geometries. The higher ratio of B_{12} to A_{12} for the trilayer on GaAs resulted in a greater high-field curvature than for the trilayer on sapphire. The models of Gradmann and Elmers [24] and of Bobo et al. [20] were both recognised as providing possible alternative explanations for the high-field curvature. Two other models based on anisotropies and paramagnetic spins were discussed, but ruled out on the basis of measurements performed on the single Co layer.

(vi) Analysis of the polar saturation fields of both Cu-wedged trilayers as a function of Cu thickness allowed the positions of the AFM coupling maxima to be deduced, and showed that the period of the oscillation was 11 ± 2 Å for both trilayers, in agreement with previous reports. In addition, large variations in the perpendicular saturation field were observed which could not be attributed to exchange coupling. These variations in saturation field are believed to have revealed imperfections in the structural quality of the Cu-wedged trilayers on a long lateral length scale which could not be discerned using other measurement techniques.

(vii) NMR measurements have shown that the Co–Cu interfaces are of reasonably good quality on a short lateral length-scale. They reveal that the strength of the exchange coupling in Co/Cu(111) samples is critically dependent on the magnetic/non-magnetic interface quality and increases with an improvement in the interface quality in such samples. The poorer interface quality for the trilayer on sapphire compared with the trilayer on GaAs was shown to be consistent with the higher in-plane remanence observed for the trilayer on sapphire, but different from the NMR results obtained previously by Thomson et al. [11].

(viii) PNR measurements performed on the single Co layer on GaAs showed that a significant roughness, probably on a long lateral length scale, was present in the film. This was noted to be consistent with island growth observed by Figuera et al. in the Co/Cu layers [18] leading to pinholes in the Cu layers, and with island growth observed in the buffer/substrate structure using STM measurements. It was suggested that the roughness may also explain the occurrence of the features due to structural imperfections observed in the plots of the polar saturation fields versus Cu thickness on the Cu-wedged trilayers.

An overall picture of the coupling and magnetization behaviour in MBE-grown Co/Cu(111) structures has thus been obtained. Evidence has been found to support the presence of a significant biquadratic coupling in addition to the bilinear coupling in these samples, and to support the abundance of separate extrinsically ferromagnetically coupled regions alongside normal intrinsically exchange-coupled regions. It has been shown that the coupling and magnetization behaviour of these films depends strongly on the quality of the interfaces of the various layers. In addition, it has been shown that whereas the structures have well defined interfaces on a short lateral length scale, they appear inhomogeneous when viewed on a long lateral length scale. These features are believed to be due to the growth processes specific to MBE-grown Co/Cu(111) structures, and to be representative of the quality of sample that can be currently achieved using present growth techniques.

Acknowledgements

The authors would like to acknowledge help from C. Daboo, R.J. Hicken, and M. Patel of the University of Cambridge, and thank J. Penfold of the Rutherford Appleton Laboratory for assistance with the PNR measurements. Financial support from the Toshiba Corporation, the EPSRC, and the Newton Trust is gratefully acknowledged.

References

[1] S.S.P. Parkin, R. Bhadra and K.P. Roche, Phys. Rev. Lett. 66 (1991) 2152.

[2] S.S.P. Parkin, Z.G. Li and David J. Smith, Appl. Phys. Lett. 58 (1991) 2710.
[3] D. Greig, M.J. Hall, C. Hammond, B.J. Hickey, H.P. Ho, M.A. Howson, M.J. Walker, N. Wiser and D.G. Wright, J. Magn. Magn. Mater. 110 (1992) L239.
[4] W.F. Egelhoff Jr. and M.T. Kief, Phys. Rev. B 45 (1992) 7795.
[5] M.T. Johnson, R. Coehoorn, J.J. de Vries, N.W.E. McGee, J. aan de Stegge and P.J.H. Bloemen, Phys. Rev. Lett. 69 (1992) 969.
[6] M.A. Howson, B.J. Hickey, J. Xu, D. Greig and N. Wiser, Phys. Rev. B 48 (1993) 1322; M.A. Howson, B.J. Hickey, J. Xu, D. Greig, P. Rhodes and N. Wiser, Phys. Rev. B 49 (1994) 9560.
[7] J.P. Renard, P. Beauvillain, C. Dupas, K. Le Dang, P. Veillet, E. Vélu, C. Marliere and D. Renard, J. Magn. Magn. Mater. 115 (1993) L147.
[8] A. Schreyer, K. Bröhl, J.F. Ankner, C.F. Majkrzak, Th. Zeidler, P. Bödeker, N. Metoki and H. Zabel, Phys. Rev. B 47 (1993) 15334.
[9] C. Dupas, E. Kolb, K. Le Dang, J.P. Renard, P. Veillet, E. Vélu and D. Renard, J. Magn. Magn. Mater. 128 (1993) 361.
[10] J. Kohlhepp, S. Cordes, H.J. Elmers and U. Gradmann, J. Magn. Magn. Mater. 111 (1992) L231.
[11] T. Thomson, P.C. Riedi and D. Greig, Phys. Rev. B 50 (1994) 10319.
[12] K. Bröhl, P. Bödeker, N. Metoki, A. Stierle and H. Zabel, J. Cryst. Growth 127 (1993) 682.
[13] R. Clarke, S. Elagoz, W. Vavra, E. Schuler and C. Uher, J. Appl. Phys. 70 (1991) 5775.
[14] J.S. Lord, H. Kubo, P.C. Riedi and M.J. Walker, J. Appl. Phys. 73 (1993) 6381.
[15] T. Thomson, P.C. Riedi, K. Bröhl and P. Bödeker, J. Magn. Magn. Mater. 148 (1995) 34.
[16] Landolt-Börnstein, Numerical Data and Functional Relationships in Science and Technology, New Series, Group III, vol. 19a (Springer, Berlin, 1986) p. 45.
[17] F. Schreiber, A. Soliman, P. Bödeker, R. Meckenstock, K. Bröhl and J. Pelzl, J. Magn. Magn. Mater. 135 (1994) 215.
[18] J. de la Figuera, J.E. Prieto, C. Ocal and R. Miranda, Phys. Rev. B 47 (1993) 13043.
[19] A.J.R. Ives, R.J. Hicken, J.A.C. Bland, C. Daboo, M. Gester and S.J. Gray, J. Appl. Phys. 75 (1994) 6458.
[20] J.-F. Bobo, M. Piecuch and E. Snoeck, J. Magn. Magn. Mater. 126 (1993) 440.
[21] R.P. Erickson, K.B. Hathaway and J.R. Cullen, Phys. Rev. B 47 (1993) 2626.
[22] P. Bruno, J. Magn. Magn. Mater. 121 (1993) 248.
[23] J.C. Slonczewski, J. Magn. Magn. Mater. 126 (1993) 374.
[24] U. Gradmann and H.J. Elmers, J. Magn. Magn. Mater. 137 (1994) 44.
[25] D. Barlett, F. Tsui, D. Glick, L. Lauhon, T. Mandrekar, C. Uher and R. Clarke, Phys. Rev. B 49 (1994) 1521.
[26] R.J. Hicken, A.J.R. Ives, D.E.P. Eley, C. Daboo, J.A.C. Bland, J.R. Childress and A. Schuhl, Phys. Rev. B 50 (1994) 6143.
[27] A.J.R. Ives, PhD thesis, University of Cambridge (1995).
[28] B.N. Engel, M.H. Wiedmann, R.A. Van Leeuwen and C.M. Falco, Phys. Rev. B 48 (1993) 9894.
[29] C. Mény, P. Panissod and R. Loloee, Phys. Rev. B 45 (1992) 12269.
[30] P. Bruno and C. Chappert, Phys. Rev. Lett. 67 (1991) 1602.
[31] K. Le Dang, P. Veillet, H. He, F.J. Lamelas, C.H. Lee and R. Clarke, Phys. Rev. B 41 (1990) 12902.
[32] T. Dumelow and P.C. Riedi, Hyperfine Interactions 35 (1987) 1061.
[33] C. Mény, Université Louis Pasteur, Strasbourg, France (1995) (private communication).
[34] CRC Handbook of Chemistry and Physics, 75th edn. (1994) p. 11-140, 12-10, 12-88.
[35] G.J. Herdman, J. Penfold and C. Shackleton, Analysis Programs for Neutron Reflection Data, Rutherford Appleton Laboratory, UK (1990).
[36] P. Dubson, Michigan State University, USA (1992) (private communication).